

Article citation info:

Chen S, Zhang X, Li Q, Shen C, Shi Y. The vertical screw conveying characteristics of cohesive particle and optimization of design parameters. *Eksploracja i Niezawodność – Maintenance and Reliability* 2023; 25(1) <http://doi.org/10.17531/ein.2023.1.13>

The vertical screw conveying characteristics of cohesive particle and optimization of design parameters

Indexed by:



Suifan Chen^{a*}, Xiaomeng Zhang^a, Qipeng Li^a, Ce Shen^b, Yongchang Shi^b

^a School of Mechanical and Energy Engineering, Zhejiang University of Science and Technology, Hangzhou, 310023, China,

^b Hangzhou Huaxin Mechanical and Electrical Engineering Corporation, Ltd, Hangzhou, 310012, China.

Highlights

- The theoretical formulations are used to verify the reliability of the simulation.
- The DEM simulation is used to study conveying characteristics.
- Optimization of design parameters (rotational speed, pitch, and clearance) of a screw conveyor.
- The NSGA-II algorithm is applied to solve the multi-objective optimization model.

Abstract

The purpose of this paper is to solve the problem of low conveying efficiency and serious blade wear during vertical screw conveying of cohesive particles. Firstly, the reliability of DEM simulation was verified by comparing the simulated and theoretical values and the influence regularity of different design parameters (rotational speed, pitch, and clearance) on screw conveying characteristics were analyzed based on DEM. In addition, the effect of design parameters on the screw conveying characteristics is identified by ANOVA. Then, the multi-objective optimization model with the both of maximizing the average mass flow rate and minimizing the maximum wear depth of the blade was established using the polynomial fitting regression, which was solved by the non-dominated sorting genetic algorithm (NSGA-II). Finally, the comprehensive evaluation was used to determine the best design parameters. The above research results provide a certain reference for the study of cohesive particle's vertical screw conveying characteristics and equipment optimization design.

Keywords

discrete element method, conveying characteristics, NSGA-II, comprehensive evaluation

This is an open access article under the CC BY license (<https://creativecommons.org/licenses/by/4.0/>)

1. Introduction

The screw conveyor is a commonly used conveying equipment in ports, agriculture, chemical, mining, and food processing industries, which is adopted to ensure continuously and long-distance convey the bulk materials such as coal, barley, and wood chips, et al [12]. The screw conveying characteristics have long been studied based on DEM. For example, Owen and Cleary [14] studied the effects of different inclination angles, rotational speeds, and filling rates on the conveying velocity, mass flow rate, power consumption, and energy dissipation, and predicted the screw conveyor performance. Wang et al. [20] studied the influence of different rotational speeds and filling rates on mass flow rate, and the results indicated that mass flow rate increased with increasing rotational speed or filling rate increase. Zhao et al. [27] studied the influence of internal diameter, pitch, and rotational speed on the conveying capacity. Karwat et al. [8] studied the impact of the screw rotation speed

on the mass efficiency and power consumption under the different constructions of screw conveyor. Yuan et al. [26] proposed the vertical screw conveyor with variable screw section to improve the conveying efficiency.

In the above study of screw conveying characteristics, material properties such as shape, size and cohesion of particles, et al. were ignored. Therefore, Owen and Cleary [15] studied the effects of particle shape, particle-particle, and particle-geometry boundary friction on the conveying velocity, mass flow rate, and power consumption. Rackl and Günthner [17] investigated the conveying process of non-spherical particles in the screw conveyor, with particles being modeled by super-ellipsoids, and predicted the effect of different particle's shapes, filling rates, and rotational speeds on the particle's mass flow rate and power consumption. Govender et al. [2] studied the impact of different faced particle shapes on the energy dissipation of screw

(*) Corresponding author.

E-mail addresses:

S. Chen, 106013@zust.edu.cn, X. Zhang, 1031498008@qq.com, Q. Li, liqipeng@zust.edu.cn, C. Shen, 13305719551@189.cn, Y. Shi, 15868461267@126.com

conveyor, and the results indicated that faced particle's the energy dissipation is higher than that of spherical particles. Minglani et al. [13] investigated the influence of spherical and non-spherical particles on the average velocity and contact force at different rotational speeds, pitches, and feeding rates, the results indicated that the non-spherical particles follow a similar trend to those of spherical particles. Hou et al. [5] established the DEM model of cohesive particle flow in a screw feeder, and researched the effects of cohesive force and rotational speed on the mass flow rate and contact forces. The authors [10, 16] studied the effect of particle sizes on the conveying characteristics, such as the mass flow rate and power consumption.

To study the wear regularity of the screw blade, Yang et al. [23, 24] established a new screw conveyor wear prediction model based on the Archard wear model and the continuous medium assumption, and the wear regularity of the screw blade was simulated and experimentally verified at different rotational speeds, filling rates, and pitches.

Many papers correctly and purposefully investigated that the effects of many different design parameters on the conveying characteristics of the non-cohesive particles, such as the conveying efficiency, power consumption, and velocity of particles, et al. However, there is little research on the use of cohesive particles as conveying materials in screw conveyors, and there is a lack of paper on the combination of conveying efficiency and the blade wear. Therefore, in order to improve the conveying efficiency and reduce the blade wear of the screw conveyor with cohesive particles, a method based on the combination of DEM and NSGA-II algorithm is proposed in this paper for analysis. Firstly, the effect of different design parameters (rotational speed, pitch, and clearance) on vertical screw conveying characteristics is investigated based on DEM simulation. Then, a multi-objective optimization model of screw conveyor design parameters for viscous particles is established with rotational speed, pitch, and clearance as design variables and the objectives of maximizing conveying efficiency and minimizing blade wear. The NSGA-II algorithm is adopted to obtain the Pareto optimal solution sets. Finally, the entropy weight method combined with the grey relational method is applied for the comprehensive evaluation to determine the best design parameters of the screw conveyor equipment for cohesive particles.

2. Setup vertical screw conveyor simulation model

2.1. Simulation model

This study uses the actual model of a certain type of vertical screw conveyor in the enterprise, and in order to reduce the scale of the simulation, the model is scaled down to one third of the original one without affecting the reliability of the simulation test, then the schematic diagram of the structure of the vertical screw conveyor and the structural parameters of the scaled model are shown in Fig. 1 and Table 1. The mass flow rate monitor, velocity sensor and Geometry Bin are arranged in the monitoring area to count the mass flow rate of particles, the velocity of particles, and the wear depth of the blade, respectively.

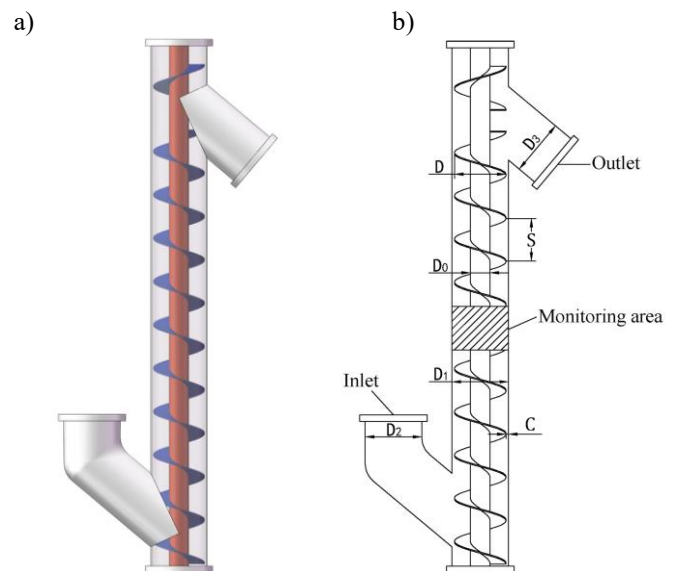


Fig. 1. The structure of vertical screw conveyor: a. three-dimensional simplified model; b. two-dimensional model.

Table 1. Design parameters of the scaled-down model.

Name and Symbol	Value
D – External diameter of the screw blade	237 mm
D_0 – Diameter of the screw shaft	91 mm
D_1 – Internal diameter of cylinder wall	250–254 mm
D_2 – Diameter of inlet	250 mm
D_3 – Diameter of outlet	250 mm
C – Clearance	6.5–8.5 mm
S – Pitch	190–237 mm
n – Rotational speed	260–360 rpm

2.2. Material parameters

The cohesive material is studied with coal particles, the radius of particle r is selected as 6 mm [25]. Meanwhile, the steel is set for the material of the vertical screw conveyor. The material parameters and contact properties of particle and steel are shown in Table 2.

Table 2. Material parameters [21, 22, 24].

Material parameters	Value
ϵ_c – Poisson's ratio of particle	0.3
ρ_c – Density of particle	1300 kg/m ³
G_c – Shear modulus of particle	1×10 ⁹ Pa
ϵ_s – Poisson's ratio of steel	0.29
ρ_s – Density of steel	7861 kg / m ³
G_s – Shear modulus of steel	7.99×10 ¹⁰ Pa
Recovery coefficient of particle-particle	0.5
Static friction coefficient of particle-particle	0.6
Rolling friction coefficient of particle-particle	0.05
Recovery coefficient of particle-steel	0.5
Static friction coefficient of particle-steel	0.4
Rolling friction coefficient of particle-steel	0.05
Wear constant of particle-steel	1×10 ⁻¹² m ² / N

The time step is determined according to the Rayleigh wave velocity propagating along the surface of a solid spherical particle, as follows in Equation (1) [7]:

$$\Delta t = \frac{\pi r}{0.163\epsilon_c + 0.877} \sqrt{\frac{G_c}{\rho_c}} \quad (1)$$

The corresponding numerical is brought in Eq. 1 to obtain $\Delta t = 2.32 \times 10^{-5}$ s. The Rayleigh time step is usually set in the time

step range of 5% to 40%. Therefore, the simulation time step is set to 4.64×10^{-6} s, and the total simulation time is set to 10s, with data saved every 0.05s [24].

2.3. Selection of particle contact model

The current moisture content of commercially available coal particles is 5% to 15%, and the Hertz-Mindlin with JKR contact model is selected to simulate wet particles [18, 21]. The corresponding force-displacement control equations for this model are as follows [4]:

$$F_n = m^* \frac{d^2 \delta_n}{dt^2} - (F_n^d + F_n^s - F_n^{jkr}) \quad (2)$$

$$F_t = m^* \frac{d^2 \delta_t}{dt^2} - (F_t^d + F_t^s) \quad (3)$$

$$I^* \frac{d^2 \theta}{dt^2} = M_c + M_r \quad (4)$$

Where, F_n is the normal external force, F_t is tangential external force, m^* is the equivalent mass, I^* is the equivalent moment of inertia, δ_n is the normal displacement, δ_t is the tangential displacement, M_c is the sum of a contact torque, M_r is rolling resistance torque, θ is the angle of particle rotation, F_n^d is the normal damping force, F_t^d is the tangential damping force, F_n^{jkr} is the normal cohesive force, F_n^s is the normal spring force, F_t^s is the tangential spring force.

Here, F_n^d , F_n^{jkr} , F_n^s , F_t^d , F_t^s can be expressed as [4]:

$$F_n^d = -2 \sqrt{\frac{5}{6} \frac{lne}{\sqrt{\ln^2 e + \pi^2}} \sqrt{2E^* \sqrt{r^* \delta_n m^*}} \frac{d\delta_n}{dt}} \quad (5)$$

$$F_n^{jkr} = 4 \sqrt{\pi \gamma a^3 E^*} \quad (6)$$

$$F_n^s = -\frac{4E^* a^3}{3r^*} \quad (7)$$

$$F_t^d = -2 \sqrt{\frac{5}{6} \frac{lne}{\sqrt{\ln^2 e + \pi^2}} \sqrt{8G^* \sqrt{r^* \delta_n m^*}} \frac{d\delta_t}{dt}} \quad (8)$$

$$F_t^s = \sqrt{8G^* \sqrt{r^* \delta_n m^*}} \quad (9)$$

Where, γ is the inter-particle of cohesive energy, a is the contact radius, e is the recovery coefficient, E^* is the equivalent elastic modulus, r^* is the equivalent particle radius, G^* is the equivalent of shear modulus.

2.4. Calibration of inter-particle cohesive energy

The actual situation of coal particles at a moisture content of 10%, after experimental measurement of its angle of repose is 27° [21]. The simulation often uses the cylindrical method to calibrate inter-particle cohesive energy, add a certain amount of particles to the cylinder, and after the particles are stabilized. Lift the cylinder at a constant speed; the particles collapse downward due to the action of gravity and eventually form a stacking angle. The angle of repose is calculated as shown in Equation (10), and the experimental procedure of inter-particle cohesive energy simulation calibration is shown in Fig. 2.

$$\beta = \arctan \frac{H}{p} \quad (10)$$

Where, β is the angle of repose; H is the particle stacking height; p is the particle stacking radius.

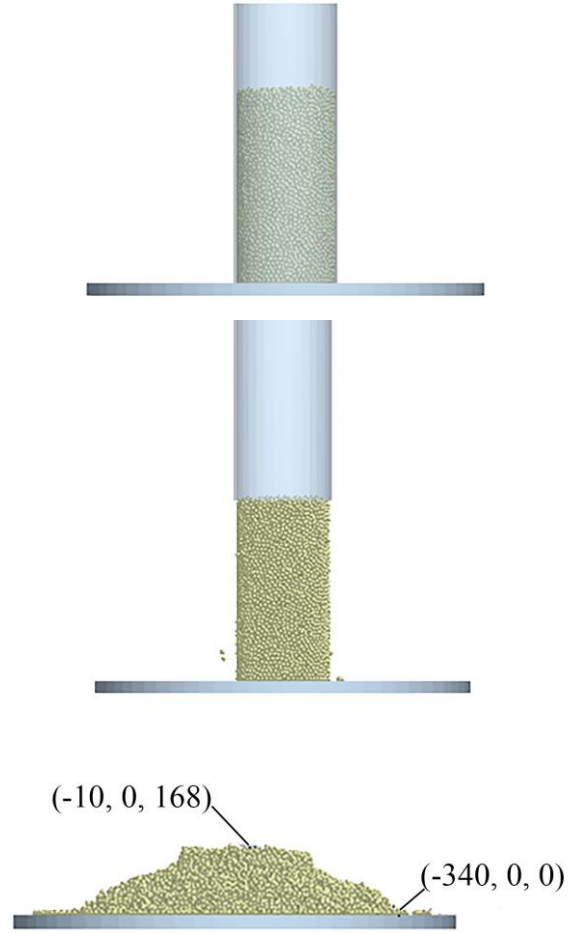


Fig. 2. Simulation calibration process.

Fig. 2 shows the particle stacking height is 168 mm, the radius of the pile is 330 mm, and the coal particle's angle of repose is 26.98° , calculated by Equation (10), which is approximately the same as the actual particle's angle of repose. At this time, the inter-particle cohesive energy is 30 J/m^2 .

Under cohesive particles, to study the effect of different design parameters on the screw conveying characteristics, the set of numerical simulation design parameters is shown in Table 3.

Table 3. Setting of design parameters.

Name and symbol	Value
Rotational speed n [rpm]	260, 285, 310, 335, 360
Pitch (S) [mm]	190, 200, 210, 220, 230, 237
Clearance (C) [mm]	6.5, 7, 7.5, 8, 8.5
Inlet feeding rate [kg/s]	4
Inlet declining speed [m/s]	2
Inter-particle cohesive energy γ [J/m^2]	30

3. Analysis of discrete element simulation results

3.1. Simulation rationality verification

When there is no adhesion energy inter-particle (0 J/m^2), according to the theoretical formula, the axial velocity of particles v_z is as follows [11]:

$$v_z = \frac{\pi R}{60} (n - n_k) \sin [2 \arctan \frac{S}{2\pi R}] \quad (11)$$

$$n_k = \frac{30}{\pi} \sqrt{\frac{g}{\mu_t R} \tan [\arctan (\frac{S}{2\pi R}) + \varphi_k]} \quad (12)$$

Where, v_z is the axis velocity of particles, n is the actual rotational speed, g is the acceleration of gravity, R is the external

radius of screw blade, the friction coefficient of particles and internal cylinder wall μ_t is 0.4, the friction angle of particle and screw blade φ_k is 21.77° [24].

When the pitch is 200 mm, clearance is 6.5 mm, and typical rotational speeds are 260 rpm, 310 rpm and 360 rpm, respectively, and the theoretical values of the particle's axial velocity are in Table 4. Under this conveying condition, the axial velocity distribution of particles in the monitoring area and the variation regularity of the particle's average axial velocity with time are shown in Fig. 3(a) and Fig. 3(b), respectively, using EDEM software simulation.

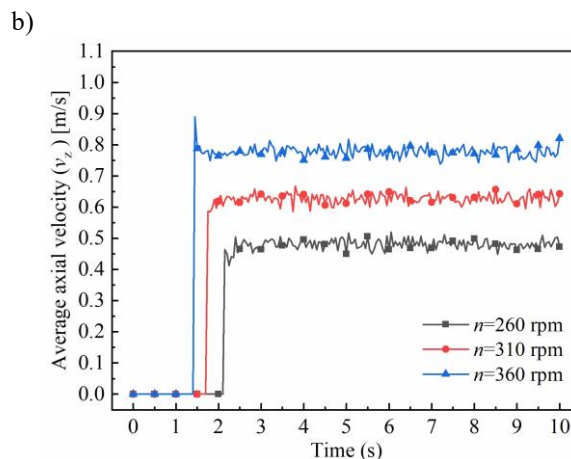
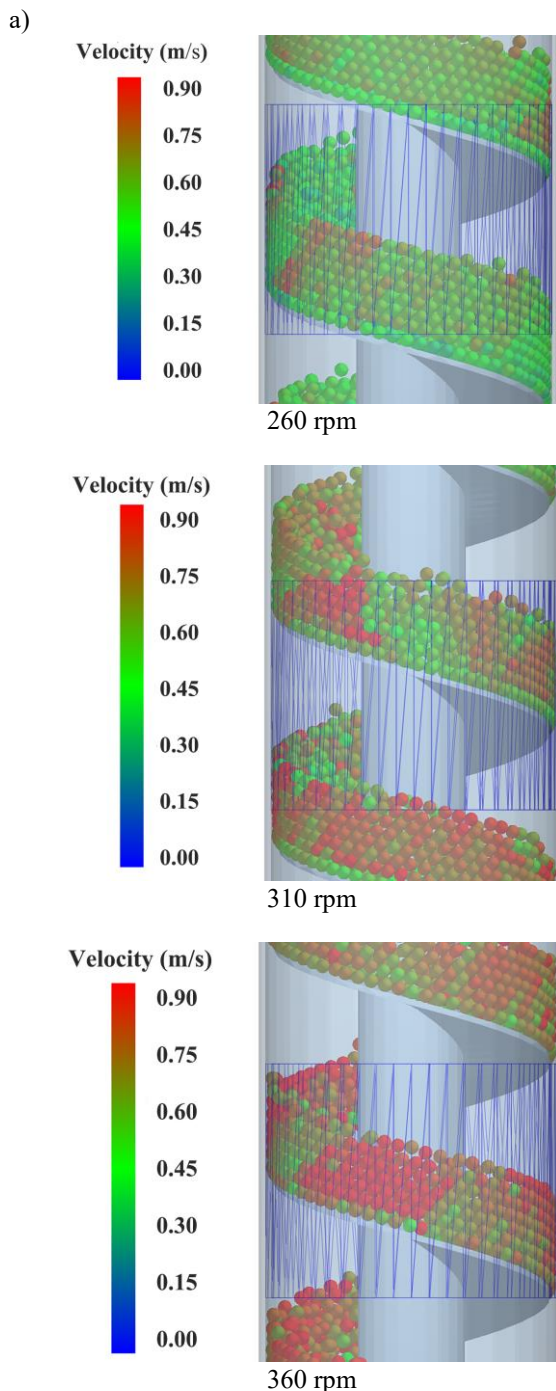


Fig. 3. At typical rotational speeds: (a) axial velocity distribution of particles; (b) the variation regularity of particles average axial velocity with time.

Fig. 3(a) shows that the axial velocity of the particles appears to have a layered distribution in the monitoring area, under the same rotational speed. The particles with lower speeds are distributed in the bottom layer, while the particles with higher speeds are primarily distributed in the middle and upper layers. Fig. 3(b) shows the average axial velocity of particles increases with the increase of the rotational speed, and the moment of particles appearance in the monitoring area are about 2.5 s, 2 s, and 1.5 s, respectively when the rotational speed is 260 rpm, 310 rpm, and 360 rpm. Also, the average axial velocity of particles at different moments is averaged in the monitoring area, and the average axial velocity of particles at typical rotational speed is obtained as follows in Table 4.

Table 4 shows the relative errors between the simulated and theoretical values of the particle's average axial velocity at typical rotational speeds are within 10%, which proves that the simulation settings are reasonable [3]

Table 4. Theoretical and simulated average axial velocity of particles.

Rotational speed n , rpm	Theoretical v_z , m/s	Simulated v_z , m/s	Relative error, %
260	0.439	0.482	9.79
310	0.594	0.628	5.72
360	0.750	0.777	3.60

3.2. The influence regularity of different design parameters on the average mass flow rate of particles

The average mass flow rate of particles is an important indicator that affects the conveying efficiency of the vertical screw conveyor [14]. In the monitoring area, the simulation studies the effect of three key parameters, namely different rotational speeds, pitches, and clearances, on the average mass flow rate of particles.

1) Rotational speed

When the inter-particle cohesive energy, pitch, and clearance are 30 J/m^2 , 200 mm, and 6.5 mm, respectively, the variation curves of the particle's mass flow rate with time at different rotational speeds are obtained using EDEM software simulation as shown in Fig. 4(a). Meanwhile, the average values of the particle's mass flow rate are calculated when the rotational speeds are 260 rpm, 285 rpm, 310 rpm, 335 rpm, and 360 rpm, respectively, and the

variation curve of the particle's average mass flow rate with rotational speed is fitted as shown in Fig. 4(b).

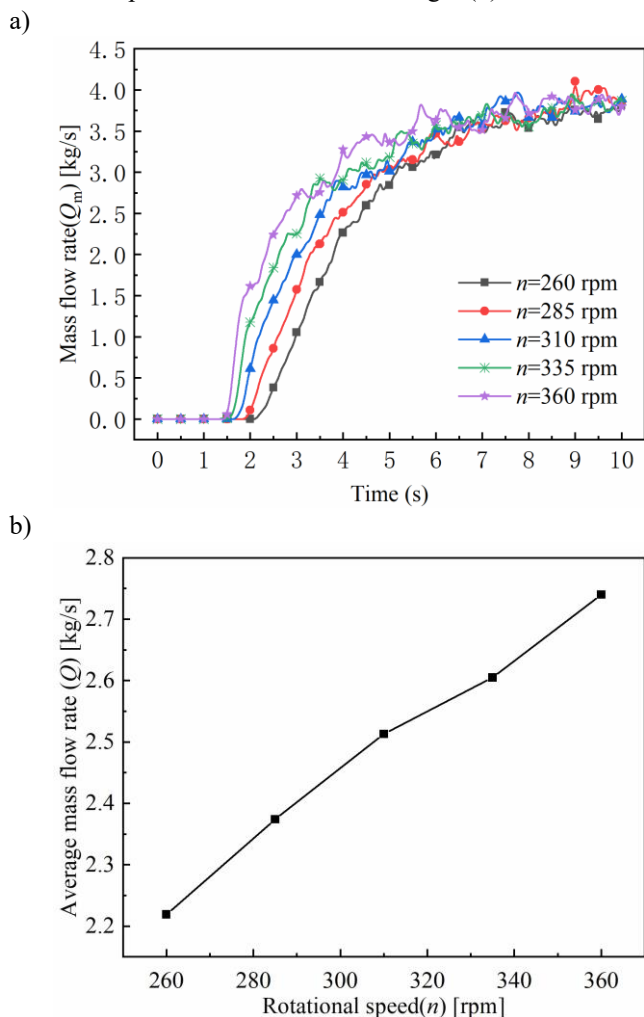


Fig. 4. At different rotational speeds: (a) Variation curves of the particle's mass flow rate with time; (b) Variation curves of particle's average mass flow rate.

Fig. 4(a) shows the particle's mass flow rate reaches the steady state at different rotational speeds are about 7s. Fig. 4(b) shows particle's average mass flow rate increases strongly with the increase in the rotational speed. The average mass flow rate of particles increases from 2.219 to 2.740 kg/s, and the growth rate of the particle's average mass flow rate is 23.48%, when the rotational speed increases from 260 to 360 rpm.

2) Pitch

When the inter-particle cohesive energy and clearance are 30 J/m^2 and 6.5 mm, respectively, the pitch increases from 190 to 237 mm, and the variation of the particle's mass flow rate with time at different pitches (rotational speed 360 rpm is selected as an example) and the variation curves of the particle's average mass flow rate with the pitch at three typical rotational speeds are obtained by using EDEM software simulation, as shown in Fig. 5(a) and Fig. 5(b).

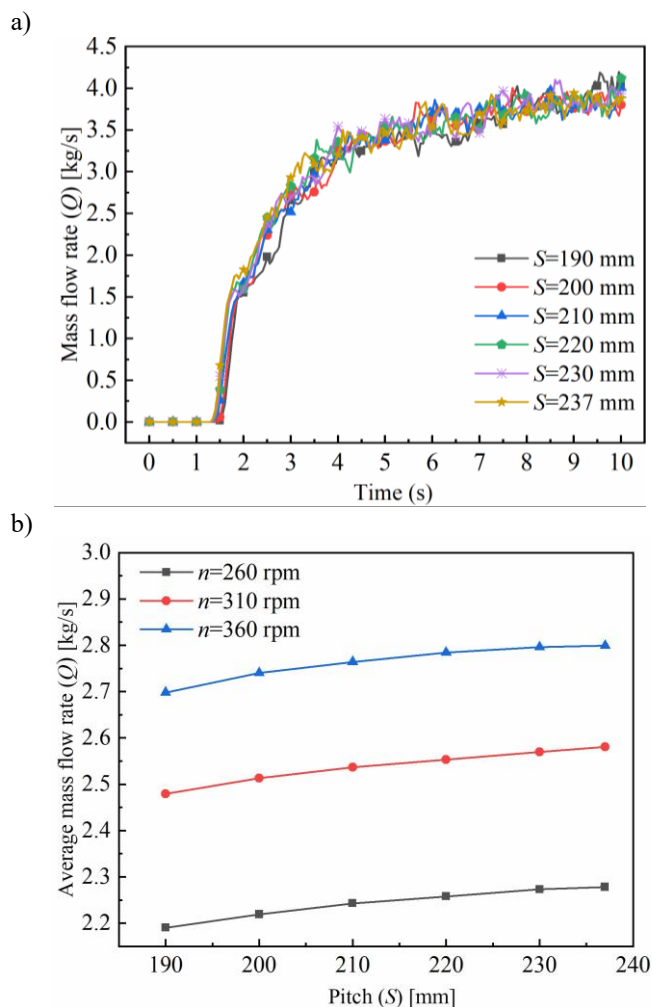


Fig. 5. At different pitches: (a) Variation curves of the particle's mass flow rate with time; (b) Variation curves of the particle's average mass flow rate (three typical rotational speeds).

Fig. 5(a) shows that the particle's mass flow rate reaches the steady state at different pitches at about 7s. Fig. 5(b) shows the average mass flow rate of particles increases with the increase in the pitch at the same rotational speed. The particle's average mass flow rate increases from 2.190 kg/s, 2.479 kg/s, and 2.698 kg/s to 2.278 kg/s, 2.581 kg/s, and 2.799 kg/s, respectively, at three typical rotational speeds (260 rpm, 310 rpm and 360 rpm), when the pitch increases from 190 to 237 mm. Meanwhile, the growth rate of the particle's average mass flow rate is about 4%.

3) Clearance

When the inter-particle cohesive energy and pitch are 30 J/m^2 and 200 mm, respectively, the clearance increases from 6.5 to 8.5 mm, and the variation of the particle's mass flow rate with time at different clearances (rotational speed 360 rpm is selected as an example) and the variation curves of the particle's average mass flow rate with clearance at three typical rotational speeds are obtained by using EDEM software simulation, as shown in Fig. 6(a) and Fig. 6(b).

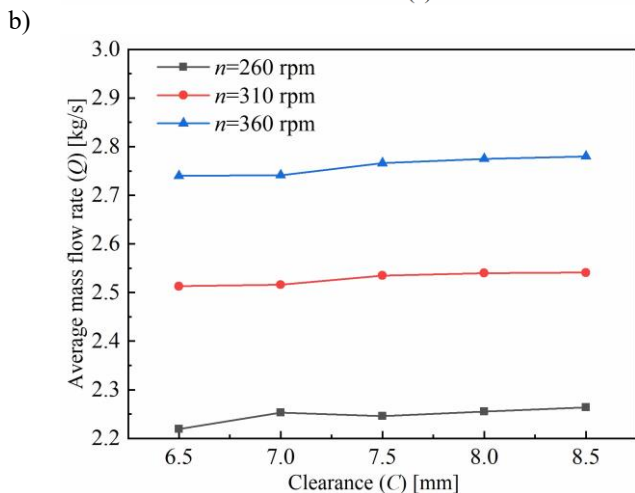
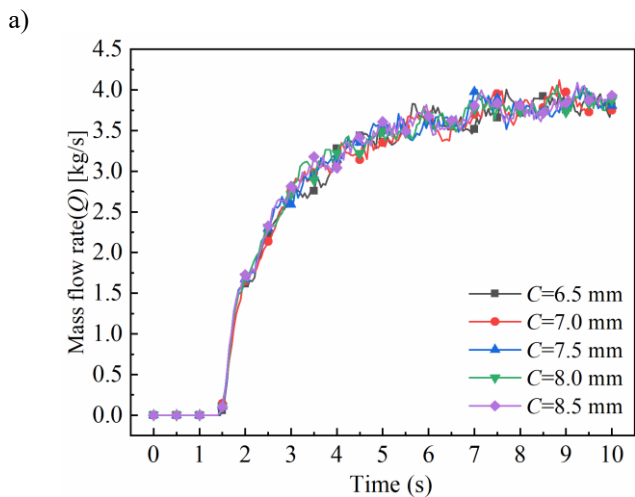


Fig. 6. At different clearances: (a) Variation curves of the particle's mass flow rate with time; (b) Variation curves of the particle's average mass flow rate (three typical rotational speeds).

Fig. 6(a) shows the particle's mass flow rate reaches the steady state at different clearances is about 7s. Fig. 6(b) shows that particle's average mass flow rate increases slightly, with the increase in the clearance at the same rotational speed. The particles average mass flow rate increases from 2.219 kg/s, 2.498 kg/s, and 2.739 kg/s to 2.254 kg/s, 2.531 kg/s, and 2.768 kg/s, respectively, at three typical rotational speeds (260 rpm, 310 rpm and 360 rpm), when the clearance increases from 6.5 mm to 8.5 mm. At the same time, the growth rate of the particle's average mass flow rate is about 1%.

3.3 The influence regularity of different design parameters on the blade maximum wear depth

In the process of screw conveying, the screw blade wears out due to collision with particles. If the screw blade occurs serious wear, it will lead to particles cannot be conveyed [23]. The variation regularity of rotational speed, pitch, and clearance on the maximum wear depth of the blade are studied, respectively based on the Archard wear model.

1) Rotational speed

When the inter-particle cohesive energy, pitch, and clearance are 30 J/m², 200 mm, and 6.5 mm, respectively, the cloud graph of blade wear degree at three typical rotational speeds is obtained by using EDEM software simulation, as shown in Fig. 7(a). At the same time, the maximum wear depth of the blade is

at the rotational speed of 260 rpm, 285 rpm, 310 rpm, 335 rpm, and 360 rpm are calculated, and the variation curve of the blade maximum wear depth with rotational speed is fitted as shown in Fig. 7(b).

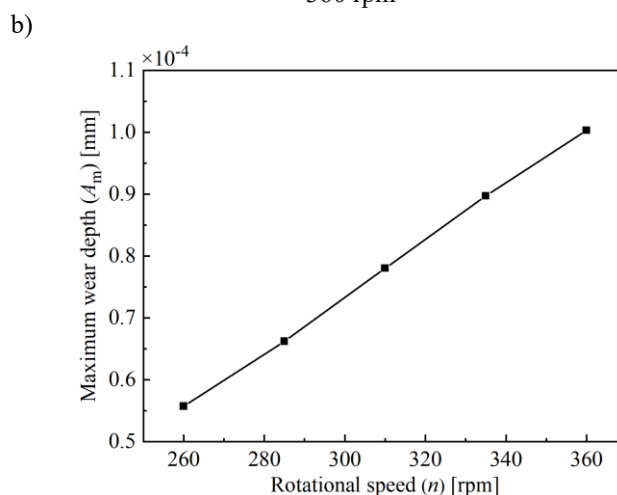
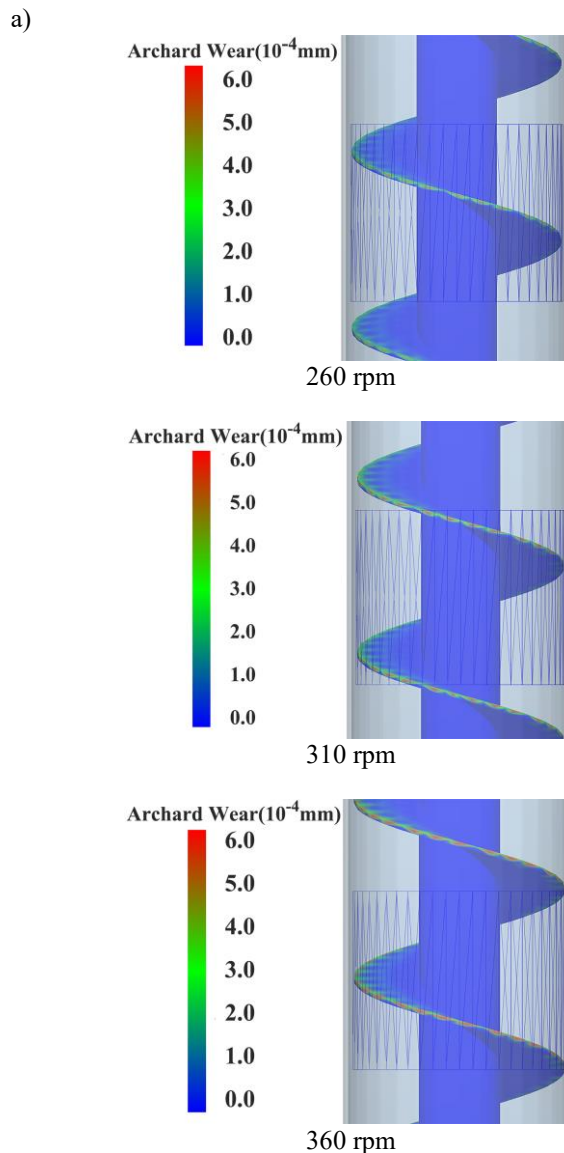


Fig. 7. (a) The cloud graph of the blade wear degree at three typical rotational speeds; (b) The variation curve of the blade maximum wear depth with rotational speed.

Fig. 7(a) shows the degree of blade wear increases with the increase in the rotational speed, and the wear is most obvious at

the edge of the blade. Fig. 7(b) shows the maximum wear depth of the blade increases strongly with the increase in the rotational speed. The maximum wear depth of the blade increases from 0.557×10^{-4} to 1.003×10^{-4} mm, and the maximum wear depth growth rate of the blade is 80.07%, when the rotational speed increases from 260 to 360 rpm.

2) Pitch

When the inter-particle cohesive energy and clearance are 30 J/m^2 and 6.5 mm, and the pitch increases from 190 to 237 mm, the EDEM software simulation is used to obtain the blade maximum wear depth with the pitch at typical rotational speeds are shown in Fig.8.

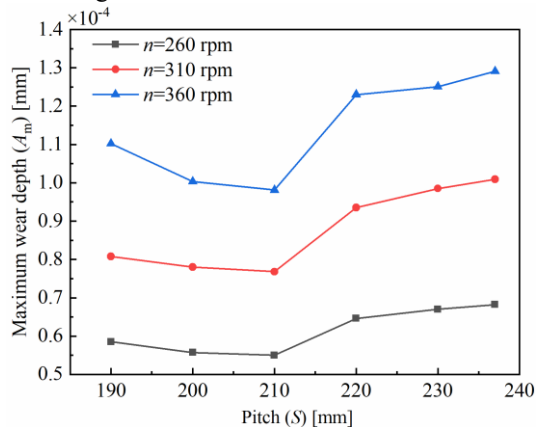


Fig. 8. Variation curve of the blade maximum wear depth with the pitch at typical rotational speeds.

Fig. 8 shows that the blade maximum wear depth decreases and then increases, with the increase in the pitch, at the same rotational speed. The maximum wear depth of the blade increases from 0.585×10^{-4} mm, 0.808×10^{-4} mm, and 1.102×10^{-4} mm to 0.682×10^{-4} mm, 1.009×10^{-4} mm, and 1.291×10^{-4} mm, respectively, at three typical rotational speeds (260 rpm, 310 rpm, and 360 rpm), when the pitch increases from 190 to 237 mm. At the same time, the maximum wear depth growth rates are 16.58%, 24.88%, and 17.15%, respectively.

3) Clearance

The inter-particle cohesive energy and pitch are set to 30 J/m^2 and 200 mm, respectively, and the clearance changes between 6.5 mm and 8.5 mm. The EDEM software simulation is used to obtain the variation curve of the blade maximum wear depth with clearance at three typical rotational speeds, as shown in Fig. 9.

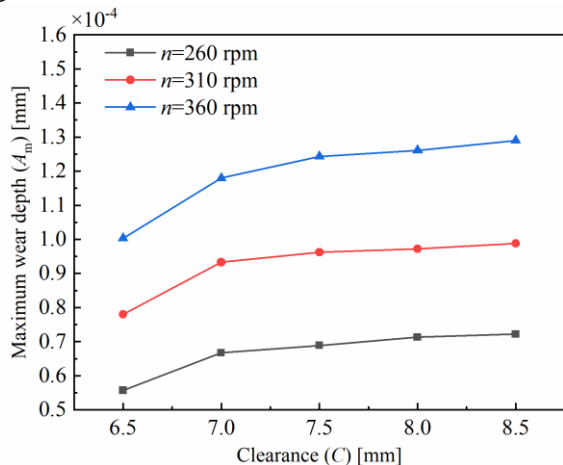


Fig. 9. Variation curve of the blade maximum wear depth with clearance at typical rotational speeds.

Fig. 9 shows that the blade maximum wear depth increases, with the increase in the clearance, at the same rotational speed. The blade maximum wear depth increases from 0.557×10^{-4} mm, 0.780×10^{-4} mm, and 1.003×10^{-4} mm to 0.722×10^{-4} mm, 0.988×10^{-4} mm, and 1.290×10^{-4} mm, respectively, at three typical rotational speeds (260 rpm, 310 rpm, and 360 rpm), when the clearance increases from 6.5 to 8.5 mm. Meanwhile, the maximum wear depth growth rates are 29.62%, 26.67%, and 28.61%, respectively.

4. Multi-objective model optimization

4.1. Construction of the regression equations

According to the above design parameters range, three horizontal parameters are selected as X1 (rotational speed) of 260 rpm, 310 rpm, and 360 rpm, X2 (pitch) of 190 mm, 213.5 mm, and 237 mm, and X3 (clearance) of 6.5 mm, 7.5 mm, and 8.5mm. Fifteen groups of simulation schemes are designed by Box-Behnken, and the simulation schemes and results are shown in Table 5.

Table 5. Box-Behnken simulation schemes and results.

Run	X1 (rpm)	X2 (mm)	X3 (mm)	Q (kg/s)	A _m (10 ⁻⁴ mm)
1	260	190	7.5	2.208	0.683
2	360	190	7.5	2.727	1.210
3	260	237	7.5	2.327	0.869
4	360	237	7.5	2.831	1.553
5	260	213.5	6.5	2.242	0.577
6	360	213.5	6.5	2.777	1.076
7	260	213.5	8.5	2.301	0.830
8	360	213.5	8.5	2.832	1.545
9	310	190	6.5	2.479	0.808
10	310	237	6.5	2.581	1.009
11	310	190	8.5	2.513	0.976
12	310	237	8.5	2.625	1.242
13	310	213.5	7.5	2.558	1.078
14	310	213.5	7.5	2.576	1.057
15	310	213.5	7.5	2.567	1.046

The regression equation for the particle's average mass flow rate is obtained by fitting a polynomial to the data in Table 5.

The regression equation $Q(X1, X2, X3)$ is as follows:

$$\begin{aligned}
 Q(X1, X2, X3) = & -2.28582 + 0.012905X1 + 0.014984 \\
 & * X2 + 0.028112 * X3 \\
 & - 3.1915 \times 10^{-6} * X1 * X2 \\
 & - 0.00002 * X1 * X3 + 0.000106 \\
 & * X2 * X3 - 0.000011 * X1^2 \\
 & - 0.000029 * X2^2 - 0.001375 \\
 & * X3^2
 \end{aligned} \quad (13)$$

The regression equation for the blade maximum wear depth $A_m(X1, X2, X3)$ is as follows:

$$\begin{aligned}
 A_m(X1, X2, X3) = & -1.81331 - 0.009169 * X1 \\
 & - 0.005057 * X2 + 0.750307 * X3 \\
 & + 0.000033 * X1 * X2 + 0.00108 \\
 & * X1 * X3 - 0.062982 * X3^2
 \end{aligned} \quad (14)$$

For the fitted regression equation for ANOVA, the degree of deviation between predicted and simulated values and the degree of influence of different parameters on the target quantities are

shown in Fig.10 and Fig. 11, respectively.

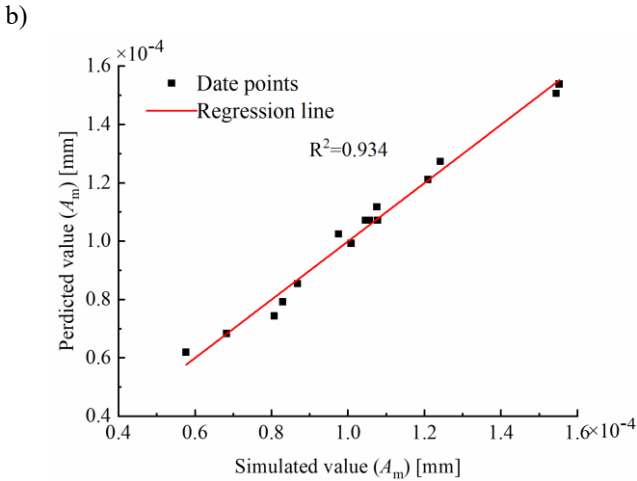
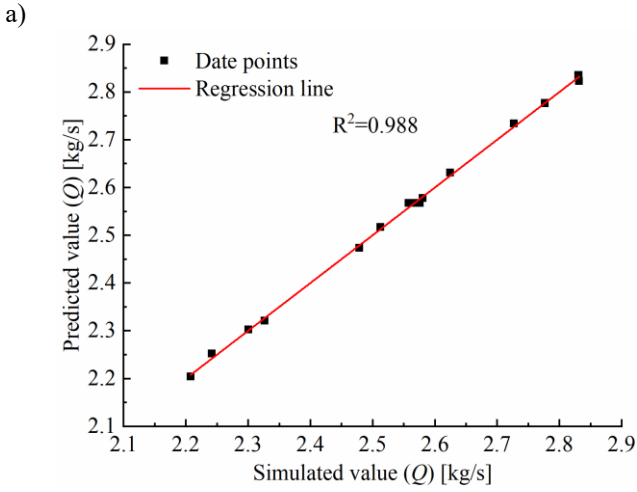


Fig. 10. The degree of deviation between the simulated and predicted values: (a) The average mass flow rate of particles; (b) The maximum wear depth of the blade.

Fig. 10(a) and Fig. 10(b) show that the data points are roughly distributed on the regression line, and the R^2 values are 0.988 and 0.934, respectively. The closer the R^2 value is to 1, the better the regression equation is fitted, indicating that the accuracy of the function model for different objectives meets the requirements [6].

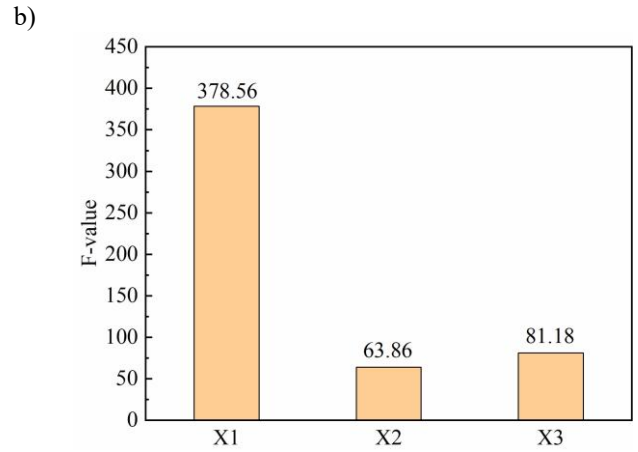
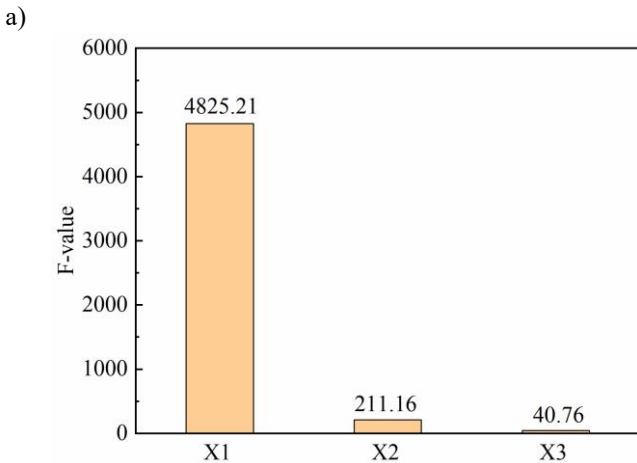


Fig. 11. F-value of each parameter at different objective quantities: (a) The average mass flow rate of particles; (b) The maximum wear depth of the blade.

Fig. 11(a) shows the magnitude of F-value in the order of X1, X2, and X3, and Fig. 11(b) shows the magnitude of F-value in the order of X1, X3, and X2. The larger F-value of the corresponding parameter, the greater the influence on the objective quantity [9]. The order of impact on the average mass flow rate of particles which is rotational speed, pitch, and clearance, and the order of influence on the maximum wear depth of the blade which is rotational speed, clearance, and pitch.

4.2. Establish multi-objective model and NSGA-II algorithm solution

In order to solve the composite problem of maximizing the average mass flow rate of particles and minimizing the maximum wear depth of the blade during vertical screw conveying under the constraints of multiple design variables. The NSGA-II algorithm is adopted to find the optimization of the established multi-objective model. The multi-objective optimization model is as follows in Equation (15), and the NSGA-II algorithm process is shown in Fig. 12.

$$\begin{cases} \text{Max}Q(X1, X2, X3) \\ \text{Min}A_m(X1, X2, X3) \end{cases} \quad (15)$$

$$s. t. \begin{cases} 260 \leq X1 \leq 360 \\ 190 \leq X2 \leq 237 \\ 6.5 \leq X3 \leq 8.5 \end{cases}$$

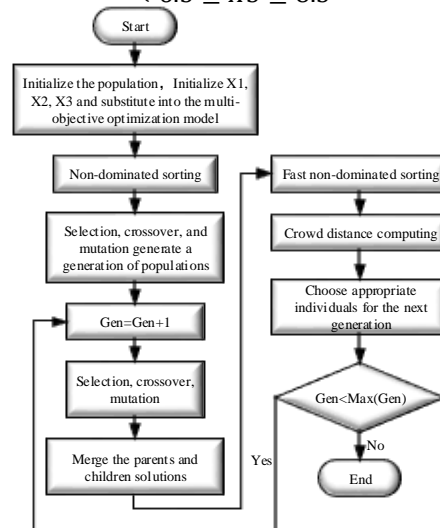


Fig. 12. The process of NSGA-II algorithm.

The parameters of the NSGA-II algorithm are set: the initialized population is 48, the maximum number of iterations is 500, the crossover probability is 0.8, the mutation probability is 0.05, the crossover distribution index is 20, and the variance distribution index is 40. The NSGA-II algorithm is used to obtain the Pareto optimal solution sets, the simulated results for the target quantities corresponding to different design parameters are shown in Table 6, and the Pareto optimal solution sets are shown in Fig. 13.

Table 6. The Pareto optimal solution sets.

S. No	X1 (rpm)	X2 (mm)	X3 (mm)	Q (kg/s)	A _m (10 ⁻⁴ mm)
1	360	236.5	8.5	2.876	1.631
2	260	190	6.5	2.190	0.513
3	360	216.8	6.5	2.798	1.108
4	360	234.4	6.5	2.823	1.228
5	360	234.4	8.3	2.869	1.601
6	360	200.2	6.6	2.760	1.026
·					·
·					·
·					·
46	360	224.1	7.8	2.843	1.468
47	360	236.5	6.5	2.825	1.243
48	360	236.5	6.6	2.828	1.274

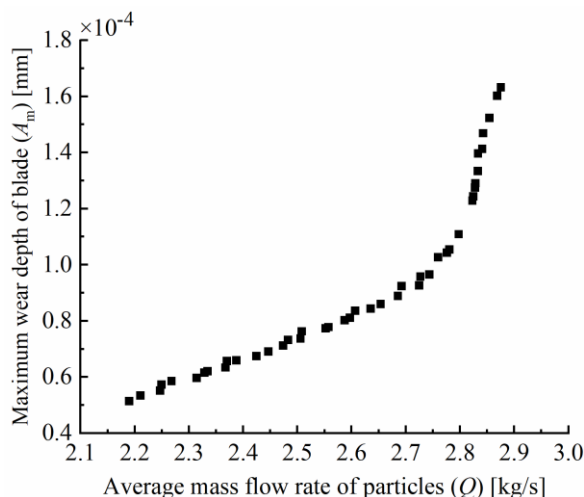


Fig. 13. The distribution of Pareto optimal solution sets at different conveying.

4.3. Comprehensive evaluation

The entropy weight method [1] combined with the grey relational method [19] is used for the comprehensive evaluation to determine the optimal conveying condition in the Pareto optimal solution sets. Firstly, the data in Table 6 are normalized and converted to dimensionless form. Forward and reverse normalization are shown in Equations (16) and (17), respectively.

$$y_i^*(j) = \frac{y_i(j) - y_i(j)_{\min}}{y_i(j)_{\max} - y_i(j)_{\min}} \quad (16)$$

$$y_i^*(j) = \frac{y_i(j)_{\max} - y_i(j)}{y_i(j)_{\max} - y_i(j)_{\min}} \quad (17)$$

Where, $y_i^*(j)$ is normalized data of the i th conveying condition for the j th indicator; $y_i(j)_{\max}$ and $y_i(j)_{\min}$ are the maximum and minimum values of the i th conveying condition for the j th indicator, respectively.

The data standardization of the particle's average mass flow rate and the blade maximum wear depth are calculated according to Equations (16) and (17), respectively, and the standardized results are obtained as shown in Table 7.

Table 7. The normalized results.

S. No	Original data		Normalization	
	Q (kg/s)	A _m (10 ⁻⁴ mm)	Q	A _m
1	2.876	1.631	1.000	0.000
2	2.190	0.513	0.000	1.000
3	2.798	1.108	0.886	0.468
4	2.823	1.228	0.923	0.360
6	2.869	1.601	0.990	0.027
·				·
·		...		·
·				·
46	2.843	1.468	0.952	0.146
47	2.825	1.243	0.926	0.347
48	2.828	1.274	0.930	0.319

Then, the entropy weighting method is applied to determine the weight values of each indicator, as shown in Equations (18) to (20) [1]:

$$P_{ij} = \frac{y_i^*(j)}{\sum_{i=1}^b y_i^*(j)} \quad (18)$$

$$e_j = -\frac{1}{\ln b} \sum_{i=1}^b P_{ij} \ln(P_{ij}) \quad (19)$$

$$g_j = 1 - e_j \quad (20)$$

$$\omega_j = \frac{g_j}{\sum_{j=1}^k g_j} \quad (21)$$

Where, P_{ij} is contribution of the i th conveying condition for the j th indicator; e_j is entropy value for the j th indicator; g_j is variability coefficient for the j th indicator; ω_j is weight for the j th indicator; b is the number of conveying conditions; k is the number of the indicators.

Through the above formula, the weight of the particle's average mass flow rate is 0.529, and the weight of the blade's maximum wear depth is 0.471.

Finally, the grey relational method is applied to determine the relational grade of the Pareto optimal solution sets. The relational grade measures the merit of conveying condition; the higher the grade of the relational, the better the conveying condition. The equations of relational coefficient and relational grade are as follows [19]:

$$\lambda_i(j) = \frac{\Delta_{\min} + \varepsilon * \Delta_{\max}}{\Delta y_i^*(j) + \varepsilon * \Delta_{\max}} \quad (22)$$

$$\lambda_i = \frac{1}{k} \sum_{j=1}^k \omega_j \lambda_i(j) \quad (23)$$

Where, $\lambda_i(j)$ is relational coefficient of the i th conveying condition for the j th indicator; $\Delta_{\min} = \min\{\text{abs}\{\max[y_i^*(j)] - y_i^*(j)\}\}$, $\Delta_{\max} = \max\{\text{abs}\{\max[y_i^*(j)] - y_i^*(j)\}\}$, $\Delta y_i^*(j) = \text{abs}\{\max[y_i^*(j)] - y_i^*(j)\}$; ε is the distinguishing coefficient, $\varepsilon \in [0,1]$, usually take 0.5.

For the normalized data in Table 7, the relational coefficients and relational grades of the different indicators are calculated according to equations (22) and (23), as shown in Table 8.

Table 8 shows the maximum relational grade value of S. No1 is 0.343. It can be seen that the best vertical screw design parameters are rotational speed is 360 rpm, pitch is 236.5 mm, and clearance is 8.5 mm.

Table 8. Relational coefficient and Relational grade of different indicators.

S. No	Relational coefficient		Relational grade
	Q	A_m	
1	1.000	0.333	0.343
2	0.333	1.000	0.324
3	0.814	0.484	0.329
4	0.867	0.439	0.332
5	0.980	0.339	0.339
6	0.747	0.521	0.320
.
.
.
46	0.912	0.369	0.328
47	0.871	0.434	0.332
48	0.877	0.423	0.332

5. Conclusions

The influence regularity of three design parameters (rotational speed, pitch, and clearance) on the average mass flow rate of particles and the maximum wear depth of the blade is analyzed by simulation based on the Discrete Element Method (DEM), and the regression equations for the average mass flow rate of particles and the maximum wear depth of blade are analyzed for ANOVA. Then, the multi-objective optimization model with the both of maximizing the particle's average mass flow rate and minimizing the blade maximum wear depth is optimally solved by using the NSGA-II algorithm, and 48 Pareto optimal sets are obtained. Finally, the entropy weight method combined with the grey relational analysis is applied for the comprehensive evaluation to determine the optimal conveying condition. The main conclusions are as follows:

- When the inter-particle cohesive energy, pitch, and clearance are 30 J/m², 200 mm, and 6.5 mm, respectively, and the rotational speed increases from 260 to 360 rpm, the average mass flow rate growth rate of cohesive particles is 23.48%, and the maximum wear depth of blade growth rate is 80.07%.
- When the inter-particle cohesive energy and clearance are 30 J/m² and 6.5 mm, and the pitch increases from 190 to 237

Acknowledgements

This research was supported by the finance that National Key Research and Development Program of China (SQ2020YFF0423771); Zhejiang Science and Technology planning project (2020C01053). The authors sincerely thank the editors and reviewers, for their insight and comments which further improved the quality of this paper.

References

1. Feng Y, Fanghui Y, Li C. Improved Entropy Weighting Model in Water Quality Evaluation. *Water Resources Management* 2019; 33(6): 2049–2056, <https://doi.org/10.1007/s11269-019-02227-6>.
2. Govender N, Cleary P W, Wilke D N, Khinast J. The influence of faceted particle shapes on material dynamics in screw conveying. *Chemical Engineering Science* 2021; 243: 116654, <https://doi.org/10.1016/j.ces.2021.116654>.
3. Guo Y. Numerical simulation study of the flow characteristics of gas-solid two-phase flow in vertical screw conveyor. 2015.
4. Hærvig J, Kleinhans U, Wieland C et al. On the adhesive JKR contact and rolling models for reduced particle stiffness discrete element simulations. *Powder Technology* 2017; 319: 472–482, <https://doi.org/10.1016/j.powtec.2017.07.006>.
5. Hou Q F, Dong K J, Yu A B. DEM study of the flow of cohesive particles in a screw feeder. *Powder Technology* 2014; 256: 529–539, <https://doi.org/10.1016/j.powtec.2014.01.062>.
6. Hu C, Hou Y, Tie Y et al. Influence of Different Bonding Parameters on the Strength of CFRP Laminates with Single Lap Bonding Structure and Optimization. *JOURNAL OF MECHANICAL ENGINEERING* 2021; 57: 154–165.
7. Huang Y J, Nydal O J, Yao B. Time step criterions for nonlinear dense packed granular materials in time-driven method simulations. *Powder Technology* 2014; 253: 80–88, <https://doi.org/10.1016/j.powtec.2013.10.010>.
8. Karwat B, Rubacha P, Stańczyk E. Optimization of a screw conveyor's exploitation parameters. *Eksploatacja i Niezawodność – Maintenance and Reliability* 2021; 23(2): 285–293. <https://doi.org/10.17531/ein.2021.2.8>
9. Li Z, Liu Y, Wang H et al. Optimization of Ultrasonic Induced Germination of Saposchnikovia divaricate Seeds Based on Plackett-Burman and

mm, at three typical rotational speeds, the average mass flow rate of particles is about 4%, and the maximum wear depth growth rates are 16.58%, 24.88%, and 17.15%, respectively.

- When the inter-particle cohesive energy and pitch are 30 J/m² and 200 mm, and the clearance increases from 6.5 to 8.5 mm, at three typical rotational speeds, the growth rate of the average mass flow rate of cohesive particles is about 1.0%, and the growth rates of the maximum blade wear depth are 29.62%, 26.67%, and 28.61%, respectively.
- The average mass flow rate of cohesive particles would go up in proportion to the increase of rotational speed, pitch, or clearance, and the influence of the three on the average mass flow rate of cohesive particles is in the order of rotational speed, pitch, and clearance; In addition, the maximum wear depth of the blade would increase with the rotational speed or clearance up, but it would climb up and then decline with the increase of the pitch, and the influence of the three parameters on the maximum wear depth of the blade is in the order of rotational speed, clearance, and pitch.
- The best design parameters of cohesive particle's vertical screw conveyor that rotational speed, pitch, and clearance should be at 360 rpm, 236.5 mm, and 8.5 mm, respectively.

The above research results provide a certain reference for the study of the vertical screw conveying characteristics of cohesive materials. At the same time, the NSGA-II algorithm is found to meet both the conveying efficiency and reduce the wear of screw blade to improve the maintainability of conveying equipment. Furthermore, the subsequent study will consider setting the same filling rate as well as adding design parameters (screw shaft diameter, blade shape, inclination angle, and screw blade outer diameter, et al.) to study the screw conveying characteristics of cohesive materials in depth. At the same time, the power consumption model is introduced to make the next research on the cohesive particle screw conveyor oriented to high efficiency and energy saving.

- Box-Behnken Design. *Forest engineering* 2022; 38: 76–85.
10. McBride W, Cleary P W. An investigation and optimization of the “OLDS” elevator using Discrete Element Modeling. *Powder Technology* 2009; 193(3): 216–234, <https://doi.org/10.1016/j.powtec.2009.03.014>.
 11. Mei L, Cheng C, Fan Z. The Mechanical Research of Vertical Screw Conveyor Particle Group Based on the Radial Change of Material Speed. *Journal of Physics: Conference Series* 2021. doi:10.1088/1742-6596/1952/3/032026, <https://doi.org/10.1088/1742-6596/1952/3/032026>.
 12. Minglani D, Sharma A, Pandey H et al. Analysis of flow behavior of size distributed spherical particles in screw feeder. *Powder Technology* 2021; 382: 1–22, <https://doi.org/10.1016/j.powtec.2020.12.041>.
 13. Minglani D, Sharma A, Pandey H, Joshi J B. Analysis of flow behavior of cohesive monosized spherical and non-spherical particles in screw feeder. *Powder Technology* 2022; 398: 117049, <https://doi.org/10.1016/j.powtec.2021.117049>.
 14. Owen P J, Cleary P W. Prediction of screw conveyor performance using the Discrete Element Method (DEM). *Powder Technology* 2009; 193(3): 274–288, <https://doi.org/10.1016/j.powtec.2009.03.012>.
 15. Owen P J, Cleary P W. Screw conveyor performance: Comparison of discrete element modelling with laboratory experiments. *Progress in Computational Fluid Dynamics* 2010; 10(5–6): 327–333, <https://doi.org/10.1504/PCFD.2010.035366>.
 16. Rackl M, Günthner W A. Experimental investigation on the influence of different grades of wood chips on screw feeding performance. *Biomass and Bioenergy* 2016; 88: 106–115, <https://doi.org/10.1016/j.biombioe.2016.03.011>.
 17. Sun H, Ma H, Zhao Y. DEM investigation on conveying of non-spherical particles in a screw conveyor. *Particuology* 2022; 65: 17–31, <https://doi.org/10.1016/j.partic.2021.06.009>.
 18. Tsunazawa Y, Fujihashi D, Fukui S et al. Contact force model including the liquid-bridge force for wet-particle simulation using the discrete element method. *Advanced Powder Technology* 2016; 27(2): 652–660, <https://doi.org/10.1016/j.appt.2016.02.021>.
 19. Tzeng C J, Lin Y H, Yang Y K, Jeng M C. Optimization of turning operations with multiple performance characteristics using the Taguchi method and Grey relational analysis. *Journal of Materials Processing Technology* 2009; 209(6): 2753–2759, <https://doi.org/10.1016/j.jmatprotec.2008.06.046>.
 20. Wang S, Li H, Tian R et al. Numerical simulation of particle flow behavior in a screw conveyor using the discrete element method. *Particuology* 2019; 43: 137–148, <https://doi.org/10.1016/j.partic.2018.01.016>.
 21. Yan H, Liu Y, Li J et al. Simulation and experiment of screening performance of pulverized coal sample device based on EDEM. *Engineering Journal of Wuhan University* 2021; 54: 658–667.
 22. Yan H, Li Y, Yuan F et al. Analysis of the screening accuracy of a linear vibrating screen with a multi-layer screen mesh. *Strojnicki Vestnik/Journal of Mechanical Engineering* 2020; 66(5): 289–299, <https://doi.org/10.5545/sv-jme.2019.6523>.
 23. Yang W, Meng W, Dai X et al. Continuous medium hypothesis-based study on the screw flight wear model and wear regularity in a screw ship unloader. *Transactions of the Canadian Society for Mechanical Engineering* 2021; 45(4): 584–593, <https://doi.org/10.1139/tcsme-2020-0239>.
 24. Yang W, Meng W, Gao L et al. Analysis of the Screw Flight Wear Model and Wear Regularity of the Bulk Transport in Screw Ship Unloader. *Iranian Journal of Science and Technology - Transactions of Mechanical Engineering* 2022; 46(1): 15–29, <https://doi.org/10.1007/s40997-021-00422-8>.
 25. Yang Z, Xiaoxia S, Wenjun M. Research on the axial velocity of the raw coal particles in vertical screw conveyor by using the discrete element method. *Journal of Mechanical Science and Technology* 2021; 35(6): 2551–2560, <https://doi.org/10.1007/s12206-021-0526-z>.
 26. Yuan J, Li M, Ye F, Zhou Z. Dynamic characteristic analysis of vertical screw conveyor in variable screw section condition. *Science Progress* 2020; 103(3): 1–16, <https://doi.org/10.1177/0036850420951056>.
 27. Zhao R, Guo L, Gao W et al. Structure Optimization Design of Screw Conveyor based on EDEM. *Journal of Physics: Conference Series* 2022. doi:10.1088/1742-6596/2200/1/012002, <https://doi.org/10.1088/1742-6596/2200/1/012002>.